論文 / 著書情報
Article / Book Information

論題(和文)	Physics-Informed Wind Force Prediction and Structural Validation Part2: Structural Response Validation Using PINN-Predicted Wind Forces
Title(English)	
著者(和文)	LONG YIZHOU, 佐藤大樹, 陳引力, 田中英之
Authors(English)	LONG YIZHOU, Daiki Sato, Yinli Chen, Hideyuki Tanaka
出典 / Citation	日本建築学会関東支部研究報告集， I， ，pp. 545-548
Citation(English)	， I， ，pp. 545-548
発行日 / Pub. date	2026，3
権利情報	一般社団法人 日本建築学会

2025年度日本建築学会
関東支部研究報告集 I
2026年3月

Physics-Informed Wind Force Prediction and Structural Validation Part 2:Structural Response Validation Using PINN-Predicted Wind Forces

構造-振動

正会員 ○ LONG YIZHOU[*1] 同 佐藤 大樹[*2]
陳 引力[*3] 田中 英之[*4]

Base-Isolated Building, Nonlinear Time History Analysis, Hysteresis Curves, Ensemble Averaging, Response Validation

1 INTRODUCTION

Part 1[1] validated Physics-Informed Neural Network (PINN) predicted wind forces through time-history comparison, power spectral density (PSD) analysis, and inter-story coherence evaluation against wind tunnel reference data and AIJ standards. The physics-informed model demonstrated superior spectral consistency and spatial correlation compared to baseline CNN+LSTM approaches.

Part 2 extends validation to structural response analysis by applying predicted wind forces to a 25-story base-isolated building model featuring nonlinear elasto-plastic dampers. The primary objective is to verify whether PINN-generated forces yield displacement profiles, acceleration demands, and hysteretic energy dissipation statistically equivalent to those obtained from wind tunnel experiments.

Three key questions are addressed: (1) Do predicted forces produce base isolation hysteresis curves consistent with reference data? (2) How do ensemble-averaged displacement and acceleration profiles compare across three loading scenarios (X-direction, XY-coupled, XYZ-fully coupled)? (3) What is the statistical variability across five independent wind samples, and do predicted and reference forces exhibit equivalent uncertainty?

2 ANALYTICAL MODEL

2.1 Building Configuration

The analytical model represents a 25-story base-isolated building with total height $H = 100$ m. The structure features a square plan with dimensions $B = D = 24$ m and uniform story height $h = 4$ m. The superstructure is constructed using SM490 steel and remains elastic throughout analysis with an initial stiffness-proportional damping ratio of $\zeta = 2\%$[2].

The base isolation layer is located between the foundation and the first floor, consisting of laminated natural rubber bearings and U-shaped dampers. These devices provide both restoring stiffness and hysteretic energy dissipation, enabling significant reduction of wind-induced acceleration demands[3].In the present study, the superstructure is idealized as a linear elastic system in order to isolate the influence of wind force prediction accuracy on global structural response. This modeling assumption allows direct comparison between predicted and reference wind inputs without interference from material nonlinearity in the upper structure.

The base isolation layer governs the overall dynamic characteristics of the system under wind excitation. The combined action of laminated rubber bearings and U-shaped dampers introduces both flexibility and stable hysteretic damping, resulting in a pronounced shift of dominant vibration modes toward longer periods. Consequently, higher-mode contributions in the superstructure are effectively suppressed, and wind-induced response becomes strongly dependent on the accuracy of input force time histories applied at the isolation level.

Table 1: Structural parameters of the 25-story base-isolated building

Parameter	Unit	Value
Geometry		
Height (H)	m	100
Width (B)	m	24
Depth (D)	m	24
Story height (h)	m	4
Upper Structure		
Weight (W_u)	kN	120,796
Period (T_u)	s	2.21
Damping (ζ_u)	–	0.02
Base Isolation Layer		
Weight (W_b)	kN	12,715
Period (T_b)	s	3.9
Yield strain (δ_{by})	cm	2.79
Yield force (Q_{dy})	kN	4,640
Damper stiffness (k_d)	kN/cm	1,660
Isolator stiffness (k_f)	kN/cm	354

This configuration provides a suitable benchmark model[4),5)] for evaluating whether physics-informed wind force prediction can reliably reproduce not only force-level characteristics but also response-level phenomena such as nonlinear energy dissipation, displacement trajectory evolution, and torsional coupling effects.

2.2 Structural Parameters

Table 1 summarizes key structural parameters. The base isolation period $T_b = 3.9$ s is significantly longer than the fixed-base superstructure period $T_u = 2.21$ s, ensuring effective period shift under wind excitation.

2.3 Calculation Nodes

Structural response is evaluated at five representative locations at the base isolation layer: a center node (O) capturing global translational behavior and four corner nodes (LU, RU, LD, RD) where torsional effects are maximized. This configuration enables simultaneous assessment of translational and torsional response characteristics under multidirectional wind loading.

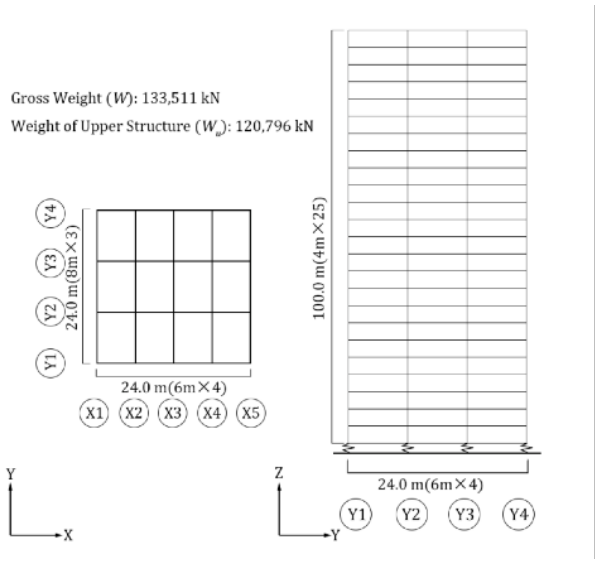

Figure 1: Building plan and elevation views

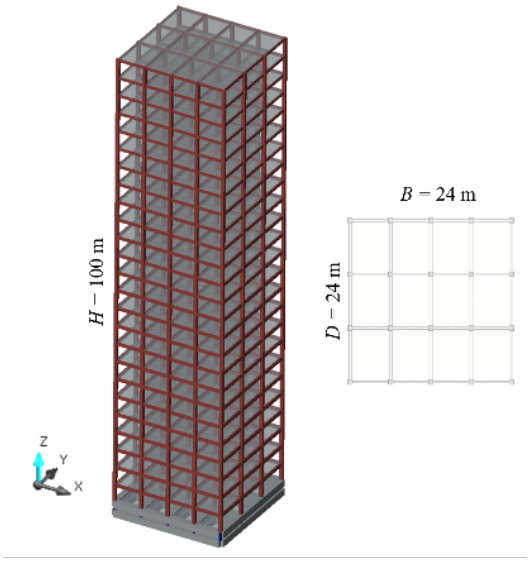

Figure 2: 3D structural model

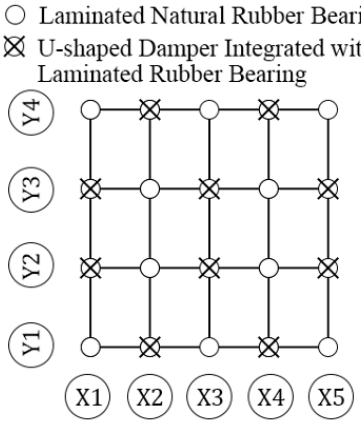

Figure 3: Base isolation device layout

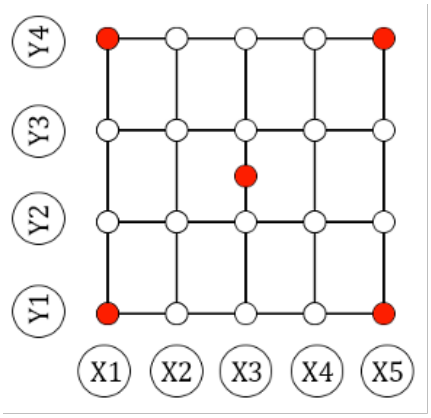

Figure 4: Calculation nodes at base isolation layer

3 STRUCTURAL RESPONSE ANALYSIS

3.1 Loading Scenarios and Analysis Method

Three loading scenarios are considered to clarify the influence of force component coupling on structural response[4),5)]. In the X case, only the along-wind force F_x is applied. The XY case includes both F_x and F_y while excluding torsional moment, and the XYZ case applies all three components simultaneously, representing realistic wind-induced excitation.

For each scenario, nonlinear time-history analyses are conducted using PINN-predicted forces, CNN+LSTM-predicted forces, and reference wind tunnel data. The equations of motion are integrated using the Newmark-β method with a time step of $\Delta t = 0.01$ s over a duration of 600 s. Ensemble averaging over five statistically independent wind samples is employed to quantify mean response trends and uncertainty.In addition to peak response evaluation, time-domain characteristics of the response are examined to assess the influence of force prediction accuracy on transient behavior. Particular attention is paid to the phase relationship between force components, as phase inconsistency may significantly affect torsional response and energy dissipation in the base isolation layer.

The ensemble-averaging procedure serves not only to reduce stochastic variability but also to evaluate the robustness of predicted wind forces. Agreement in both ensemble mean and dispersion is regarded as a necessary condition for response-level equivalence between predicted and reference inputs.

3.2 Response Metrics and Equivalence Criteria

Response-level equivalence between predicted and reference wind inputs is evaluated using complementary indices in the time domain. In addition to qualitative hysteresis comparison, peak displacement $r_{\max}$, peak acceleration $a_{\max}$, and RMS acceleration a_{rms} are extracted at representative nodes[6)], with particular emphasis on RMS response due to its relevance to serviceability assessment.

For each metric r_k obtained from the k-th wind sample ($k = 1,\ldots,5$), ensemble statistics are evaluated as

$$\mu_r = \frac{1}{5}\sum_{k=1}^{5} r_k, \qquad \sigma_r = \sqrt{\frac{1}{4}\sum_{k=1}^{5}(r_k-\mu_r)^2}. \tag{1}$$

Consistency in both μ_r and σ_r is regarded as a necessary condition for response-level equivalence[7], particularly under multidirectional coupled loading where phase inconsistency may amplify torsional demand and distort hysteretic energy dissipation.

3.3 Base Isolation Hysteresis Comparison

Figures 5 and 6 illustrate force–displacement hysteresis loops at the base isolation layer. The PINN-based results accurately reproduce yield force levels, post-yield stiffness, and unloading characteristics observed in the reference data. In contrast, CNN+LSTM-based responses exhibit reduced loop area, indicating underestimation of hysteretic energy dissipation, particularly under coupled loading conditions.For the X-direction loading case, PINN-based hysteresis loops closely follow the reference curves in terms of initial stiffness, yield onset, and loop area. This indicates that the predicted force time histories preserve both amplitude and temporal characteristics required to trigger realistic nonlinear response.

3.4 Response Profiles with Ensemble Averaging

Figures 7 and 8 compare ensemble-averaged vertical distributions of peak displacement and acceleration. PINN-based predictions show strong agreement with wind tunnel results in both mean values and standard deviation envelopes. Deviations in CNN+LSTM results increase toward upper stories, reflecting accumulated phase errors and insufficient higher-mode excitation.The vertical distribution of response reveals the cumulative effect of force prediction accuracy on structural dynamics. For displacement profiles, PINN-based results closely match reference data over the full building height, indicating appropriate reproduction of dominant vibration modes.

Acceleration profiles exhibit higher sensitivity to force prediction errors, particularly in upper stories. CNN+LSTM-based results show increased scatter and systematic deviation in acceleration demand, whereas PINN-based responses remain within the reference standard deviation range. This highlights the importance of physics-informed constraints in controlling high-frequency response components.

3.5 Base Isolation Trajectory Analysis

Figures 9 and 10 present base isolation displacement trajectories. PINN-predicted trajectories closely match reference elliptical patterns and torsional drift characteristics, whereas CNN+LSTM trajectories exhibit directional bias and reduced spatial spread, demonstrating the importance of physics-informed constraints for multidirectional response reproduction.Trajectory analysis provides an integrated representation of multidirectional response behavior. The reference trajectories exhibit elliptical patterns with clear torsional components, reflecting combined translational and rotational motion of the isolation layer.

PINN-predicted trajectories successfully reproduce these characteristics, including directional spread and orbit orientation. Conversely, CNN+LSTM-based trajectories show reduced dispersion and directional bias, indicating loss of correlation between force components. These observations confirm that physics-informed learning improves preservation of multidimensional response characteristics beyond scalar response metrics.

4 CONCLUSIONS

This study validated the effectiveness of Physics-Informed Neural Networks for predicting wind-induced structural responses of a base-isolated high-rise building. The main conclusions are as follows:

1. PINN-predicted wind forces successfully reproduced nonlinear hysteretic behavior of base isolation devices, including yield and energy dissipation characteristics.
2. Ensemble-averaged displacement and acceleration profiles obtained using PINN inputs showed strong agreement with wind tunnel results in both mean response and statistical variability.
3. Compared with conventional CNN+LSTM models, PINN demonstrated superior robustness under multi-component coupled loading, particularly in capturing torsional response features.
4. The results confirm that embedding physical constraints into deep learning frameworks significantly enhances reliability for structural response prediction under stochastic wind excitation.

REFERENCES

1. Long, Y., Sato, D., Chen, Y., Tanaka, H.: Physics-Informed Wind Force Prediction and Validation (Part 1), *AIJ Kanto Chapter Research Report Collection*, 2026. (in Japanese)
2. Tamura, Y., et al.: Evaluation of amplitude-dependent damping and natural frequency of buildings, *Eng. Struct.*, 19(9), 691-698, 1997.
3. Marukawa, H., et al.: Experimental evaluation of aerodynamic damping of tall buildings, *J. Wind Eng. Ind. Aerodyn.*, 59(2-3), 177-190, 1996.
4. ZHAO, T., Sato, D., Qian, X.: Relationship between the response of 3D model and MDOF model by using long-term wind force from typhoon simulation, *J. Struct. Eng., AIJ*, 70B, 204-210, 2024.
5. Tatsumoto, T., et al.: Evaluation of shear force by combined of wind loads in a high-rise seismically isolated building with elastic sliding bearings, *Proc. Symp. Wind Eng., AIJ*, 28, 159-166, 2024. (in Japanese)
6. AIJ: Guidelines for the Evaluation of Habitability to Building Vibration, 2004. (in Japanese)
7. Kareem, A.: Performance of multiple mass dampers under random loading, *J. Struct. Eng.*, 121(2), 348-361, 1995.

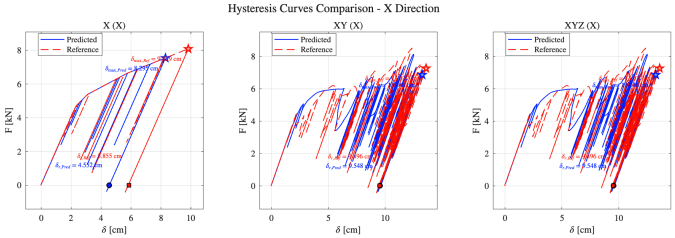

Figure 5: Hysteresis curves: X direction

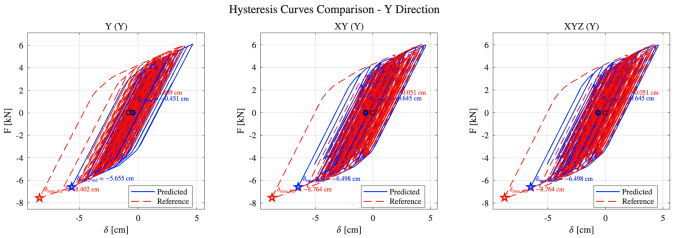

Figure 6: Hysteresis curves: Y direction

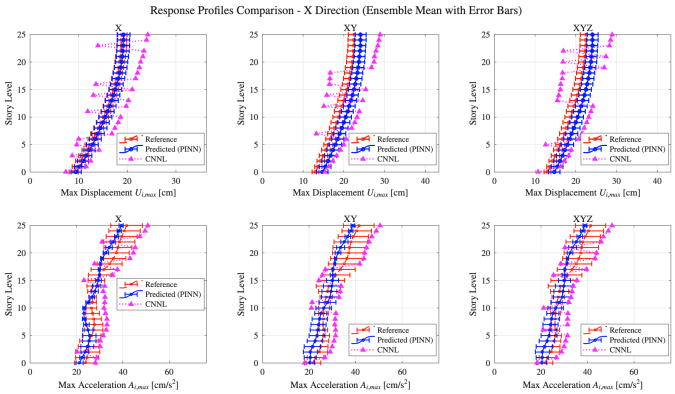

Figure 7: X-direction response profiles

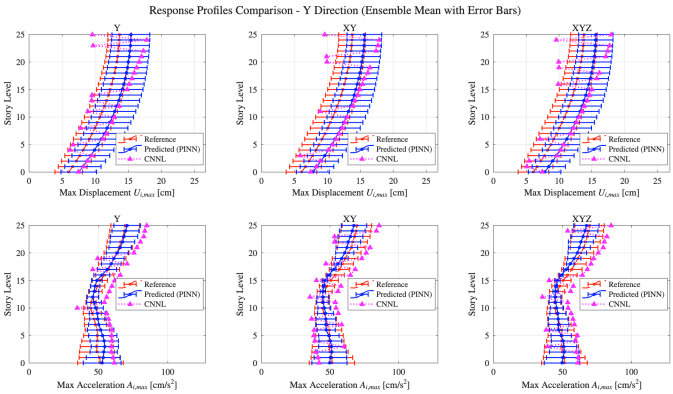

Figure 8: Y-direction response profiles

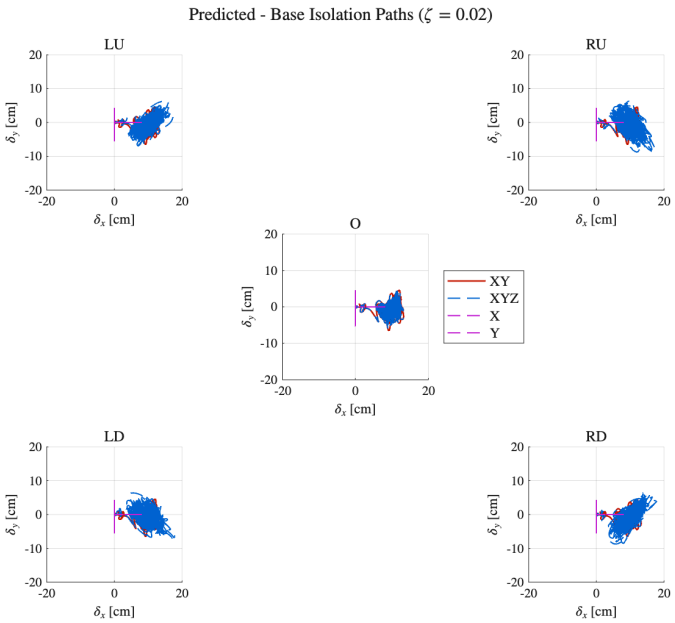

Figure 9: PINN-predicted displacement paths

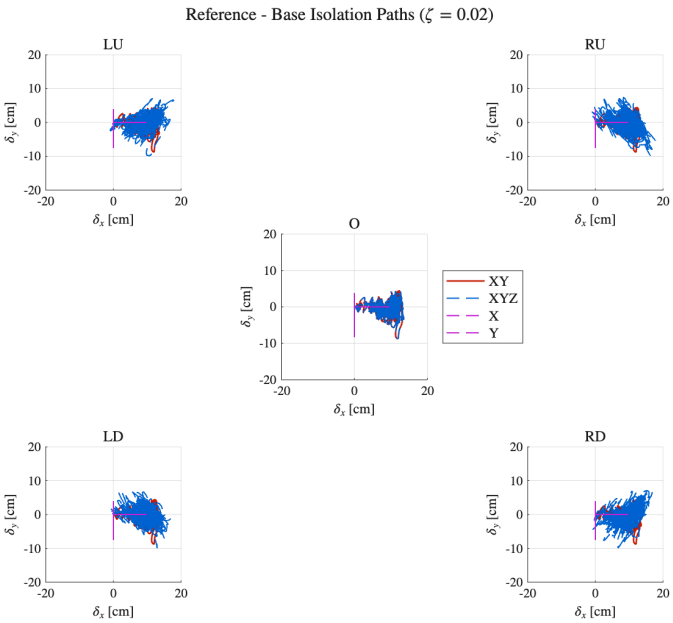

Figure 10: Reference displacement paths

*1　東京科学大学　大学院生
*2　東京科学大学　総合研究院　准教授・博士(工学)
*3　東京科学大学　総合研究院　助教・博士(学術)
*4　株式会社竹中工務店　技術研究所

Graduated Student, Institute of Science Tokyo[*1]
Associate Prof., IIR, Institute of Science Tokyo, Dr.Eng.[*2]
Assistant Prof., IIR, Institute of Science Tokyo, Ph.D.[*3]
Research & Development Institute, Takenaka Corporation[*4]